Spatial Attention-Based Adaptive CNN Model for Differentiating Dementia with Lewy Bodies and Alzheimer's Disease

K Sravani, V RaviSankar
Department of Computer Science and Engineering, GITAM University, Hyderabad, India

***Abstract*—Differentiation of Alzheimer's Disease (AD) and Dementia with Lewy Bodies (DLB) utilizing brain perfusion Single Photon Emission Tomography (SPECT) is crucial and it might be difficult to distinguish between the two illnesses. The most recently discovered characteristic of DLB for a possible diagnosis is the Cingulate Island Sign (CIS). This work aims to differentiate DLB and AD by utilizing a deep learning model and this model is named AD-DLB-DNet. Initially, the required images are collected from the benchmark dataset. Further, the Spatial Attention-Based Adaptive Convolution Neural Network (SA-ACNN) is used to visualize the CIS features from the images where the attributes are tuned using Improved Random Function-based Birds Foraging Search (IRF-BFS). Further, CIS features attained from the SA-ACNN are used to accurately differentiate the DLB and AD. Finally, the Dilated Residual-Long Short-Term Memory (DR-LSTM) layer is proposed to accurately perform the AD and DLB differentiation for identifying the clinical characteristics of the DLB. The suggested model is used for differentiating between AD and DLB for taking effective therapeutic measures. Finally, the validation is performed to validate the effectiveness of the introduced system.**

Keywords*—Alzheimer's disease and dementia with lewy bodies differentiation; spatial attention-based adaptive convolution neural network; cingulate island sign; improved random function-based birds foraging search; dilated residual-long short-term memory

I. INTRODUCTION

Global healthcare systems are severely impacted by neurodegenerative dementias, particularly as the number of elderly people rises. The World Health Organization (WHO) reports that approximately 50 million individuals globally are affected by dementia [1]. AD is responsible for around 60% of these cases, making it the most common neurological disorder [2]. DLB, characterized by the accumulation of LB, is the second most prevalent type of neurodegenerative dementia, following AD and some cases are often misdiagnosed and overlooked [3], [4]. In addition to identifying and managing clinical aspects such as severe autonomic dysfunction, motor and mental symptoms, and dangerous antipsychotic sensitivity, an accurate and timely detection of DLB is crucial for ensuring appropriate care and treatment [5].

Predicting the disease's prognosis and organizing clinical trials also depend on a reliable diagnosis, but the significant clinical and cognitive similarities between AD and DLB may make the diagnostic procedure more difficult [6]. Additionally, a variety of clinical manifestations may result from the common presence of pathological variability in individuals containing DLB, particularly the presence of co-occurring AD pathology, such as tau tangles and amyloid beta (Aβ) plaques [7]. Compared with DLB patients exhibiting solely Lewy body pathology, those with Aβ pathology is linked to reduced life expectancy and a higher rate of cognitive impairment [8]. These findings highlight the clinical significance of detecting concomitant amyloid-beta (Aβ) pathology in patients with DLB. Functional neuroimaging, a commonly employed tool in the medical detection of dementia, it has also been integrated into the detection criteria for AD as well as DLB [9], [10]. Even seasoned neurologists find it difficult to diagnose certain conditions, and sometimes choosing the best course of action is also difficult. Therefore, to give more reliable clinical evaluations, doctors employ diagnostic techniques such as neurofunctional imaging [11], [12].

Recently deep learning techniques for medical image analysis are growing steadily, particularly in neurodegenerative illnesses [13]. This broad recognition stems from its capacity to automatically identify useful features and reduce the requirement for handcrafted feature extraction. Unlike typical machine learning approaches, it can learn intricate patterns in imaging information which is difficult for humans to perceive [14], [15]. Most deep learning models used in neurodegenerative illnesses primarily identify many stages of AD, ranging from no dementia to mild AD, utilizing 2D imaging scans. Nevertheless, these models are only useful for the AD diagnosis, which means they cannot distinguish the patterns between AD and DLB. Furthermore, it is challenging to confirm their robustness when non-AD dementias are present [16], [17]. The quantitative approach requires standardized methods for acquiring and interpreting structural scans and 18F-FDG-PET, which can be time-consuming. Interestingly, in differentiating DLB from AD, a straightforward visual evaluation of Cortical Involvement (CIS) as either present or absent proved to have higher diagnostic accuracy than the quantitative CIS ratio. Although visual evaluation of other imaging indicators and modalities is widely utilized and has shown to be a quick, accurate, and repeatable procedure in clinical practice, there are no standardized visual guidelines to assess the extent of CIS. In addition to increasing the diagnostic accuracy of DLB, the use of pertinent diagnostic data may be improved using a consistent approach for classifying and interpreting the presence of CIS. Additionally, it is simple to incorporate a visual grading system into clinical practice across sites. To

effectively identify the differences between DLB and AD, a new deep learning model is introduced. The following points highlight the contributions of the developed framework.

- To develop a deep learning model to differentiate DLB from AD by utilizing images from a benchmark dataset. This approach enhances diagnostic accuracy by allowing the model to learn subtle differences between DLB and AD from high-quality, standardized brain images.
- To employ SA-ACNN to visualize and extract CIS, enabling the model to focus on the most relevant regions in medical images, thereby improving feature accuracy and relevance.
- To reintroduce BFS as IRF-BFS to fine-tune and optimize the CIS features. The parameters of SA-ACNN such as hidden neuron count, steps per epoch count, and epoch size are optimized that maximize the accuracy.
- To integrate the Dilated Res-LSTM layer, enabling the model to accurately identify and differentiate clinical features of DLB and AD, which aids in early diagnosis and effective therapeutic intervention.

The structure of the newly introduced deep learning technique for differentiating DLB and AD is outlined as follows. Section II reviews the literature on DLB and AD differentiation models. Section III presents an adaptive deep-learning mechanism designed to enhance DLB and AD differentiation, utilizing an improved optimization algorithm to boost performance and accuracy. Section IV explains the proposed model for feature extraction. Section V introduces a novel approach for differentiating DLB and AD. Part VI provides the Experimental results. Section VII contains Comparative analysis detailed discussion. Finally, Section VIII concludes the study.

II. Literature Survey

A. Related Works

In 2023, Nakata et al. [18] assessed the brain imaging variance among MCI with Lewy Bodies (MCI-LB) as well as MCI due to AD (MCI-AD) by examining brain atrophy and brain perfusion patterns. The analysis focused on differences in regional brain changes in individuals with these two conditions. It was found that MCI-LB and MCI-AD exhibited distinct patterns of brain atrophy and blood flow abnormalities. These differences helped distinguish between the two types of MCI, highlighting the unique features associated with each condition.

In 2024, Karim et al. [19] have used graph theory and machine learning measures to forecast AD. Several machine learning models were developed for AD prediction using the OASIS and SALD datasets. The study identified key elements of functional connectivity and brain network structure in AD, noting a significant loss of connections between the thalamus and top 13 regions. These findings highlighted the potential of combining machine learning, graph theory for accurate AD diagnosis and for early prediction.

In 2024, Hasan and Wagler [20] have suggested CNN-GCN architecture which was produced by first implementing the CNNs and feeding it to the GCN classifier. To train and assess the suggested techniques the whole-brain images were used. They evaluated the effectiveness of the technique by presenting the findings from the best fold out of the five folds.

In 2022, Etminani et al. [21] have developed a 3D deep learning model that utilized PET scans with a specific radioactive tracer to forecast the final clinical diagnosis of DLB, AD, and other conditions. The performance of this model was compared to that of experienced nuclear medicine physicians. To visualize the regional metabolic changes, methods were employed to highlight the areas of interest.

In 2020, Gjerum et al. [22] implemented a strong visual CIS scale and assessed its ability to distinguish between AD and DLB. When compared to AD patients and controls, DLB patients' visual CIS scores were much greater. To sum up, the visual CIS scale was a clinically helpful tool for distinguishing AD from DLB. Aβ pathology in DLB patients may be connected to the severity of CIS.

In 2020, Kanetaka et al. [23] proposed prospective research comparing the CIS on Single Photon Emission Computed Tomography (SPECT) in individuals. The CIS score, calculated using eZIS software, is the ratio of the posterior cingulate gyrus (VOI-1) to areas of notably decreased regional cerebral blood perfusion (VOI-2). Due to insignificant RCBF decline in the PCG, diagnosing MCI with the CIS score is challenging.

In 2022, Lim et al. [24] suggested a multiclass categorization technique using 3D T1-weight brain MRI images. The ResNet-50 and VGG-16 convolutional bases were utilized as feature extractors. A novel densely connected classifier was put into place to do classification on top of the convolutional bases.

In 2017, McKeith et al. [25] made a clear distinction between clinical characteristics and diagnostic biomarkers and provided guidelines on the best ways to determine and interpret them. Here, the diagnostic role of laboratory, electrophysiologic, and neuroimaging tests has been expanded. Significant progress has been made in recognizing DLB.

B. Problem Statement

Millions of people worldwide are greatly affected by the serious disorder called AD. Behavioral abnormalities and memory loss are the symptoms associated with AD. The structural changes in the brain are the main cognitive dysfunction caused by AD. To initiate the treatment approaches, dementia and AD must be detected at an earlier stage but the traditional model faces various issues, and it is listed in Table I.

Traditional strategies do not have the capability to diagnose the CIS from the images, so they fail to differentiate among the AD and DLB.

The functional connectivity of the brain is not detected by this model and this model is so invasive and costly making it unsuitable for the early diagnosis process.

TABLE I. FEATURES AND CHALLENGES OF EXISTING DLB AND AD DIFFERENTIATION MODEL

Author [citation]	Methodology	Features	Challenges
Nakata et al. [17]	RCBF	The symptoms of mild cognitive impairment are effectively detected by this model. It is used for the early AD detection.	This model fails to identify the signs of dementia.
Karim et al. [18]	SVM	This model accurately defines the structure of the brain network.	The characteristics of the brain network are not analyzed by this model.
Hasan and Wagler [19]	CNN-GCN	The initial symptoms of AD are diagnosed.	The imbalanced dataset cannot handle.
Etminani et al. [20]	3D deep learning	The systems robustness is high. The proposed model is applied in the clinical setting for making the effective decision.	The transparency of the system is low.
Gjerum et al. [21]	robust visual rating scale	The presence of dementia is effectively detected by this model. The degree of the CIS is determined by this model.	It lacks in the pathological information. The memory cohort is not analyzed by this model.
Kanetaka et al. [22]	DLB	The volume of the CIS is measured using this model.	The symptoms of the disease cannot be diagnosed.
Lim et al. [23]	CNN	It is used for executing the multi-classification of images. It uses dense connections for accurately classifying the AD in the humans.	This model does not evaluate the low-dimensional feature scores
McKeith et al. [24]	Optimal AD detection methods	It is employed to support the medical decision-making process. It is used to provide adequate medical support to the patients	The behavioral abnormalities are not detected by this model

The prior systems are ineffective for preventing the progression of DLB in individuals as they are not effectively determining the synchronization of the brain regions.

The prior approaches are unsuitable for discriminating against DLB patterns from AD patterns, so it is quite difficult to automatically detect the presence of DLB and AD from humans.

III. IMAGING CLASSIFICATION OF DEMENTIA WITH LEWY BODIES AND ALZHEIMER'S DISEASE USING DEEP LEARNING NETWORK

A. Proposed DLB and AD Imaging Classification Model: Description

Models for differentiating DLB and AD typically depend on manual feature extraction, a process that can be time-intensive and susceptible to human error. The accuracy of these models is limited due to the overlap in clinical symptoms between the two conditions. Traditional methods may not effectively capture complex patterns in neuroimaging data, leading to misdiagnosis. Additionally, these models often lack the ability to integrate and analyze multiple types of data simultaneously. Consequently, a deep learning model was developed to enhance differentiation by automatically learning and identifying intricate patterns in imaging and clinical data, improving diagnostic accuracy and efficiency. However, using deep learning for differentiating DLB and AD may face challenges including limited availability of labeled data, high variability in brain scans due to individual differences, difficulty in differentiating subtle disease patterns and so on. Thus, it is necessary to develop novel DLB and AD differentiating systems with the support of enhanced deep learning mechanism.

This study aims to differentiate DLB from AD using an advanced deep learning model. The process begins with collecting the necessary brain images from a benchmark dataset. Initially, the brain images are fed into the SA-ACNN to visualize critical image features, where SA-ACNN is developed by integrating spatial attention layer into the CNN architecture along with the network parameter optimization. For performing this optimization, an efficient heuristic algorithm named BFS is reintroduced as EBFS. Here, the parameters such as steps per epoch count, hidden neuron count, and epoch size in SA-ACNN are optimized to maximize the accuracy. The SA-ACNN's spatial attention mechanism focuses on the most relevant parts of the images, improving CIS feature extraction. Moreover, the EBFS fine-tunes this process for supporting more precise differentiation. These extracted CIS features are crucial for distinguishing between DLB and AD. The CIS involves the preservation of the Posterior Cingulate Cortex (PCC) in DLB, while hypoperfusion is typically seen in this region during the early stages of AD. The presence of the CIS has gained attention as a key differentiator, reflecting AD-related pathology that influences clinical symptoms in DLB. Notably, CIS is most prominent during the mild dementia stage and tends to decline as DLB advances. This makes CIS particularly useful for distinguishing DLB from AD, especially in the early stages, though exceptions like posterior cortical atrophy may complicate this distinction. The CIS features are then fed into the DR-LSTM for classifying DLB and AD images. This DR-LSTM combines the benefits of dilated convolutions (captures multi-scale context), and the strengths of Res-LSTM (effectively handles sequential data and long-term dependencies). Moreover, it helps in capturing detailed temporal patterns and clinical features, enhancing diagnostic capability. Thus, the DR-LSTM is expected to significantly improve the differential diagnosis of DLB and AD, enabling more effective therapeutic measures. Fig. 1 presents the pictorial presentation of the proposed DLB and AD imaging classification model.

B. Brain Image Dataset for Model Analysis

The developed framework employs brain images to differentiate DLB from AD. Table II provides a description of the dataset, which consists of images gathered from online

resources. In this context, the term $Im\,g_c^{Br}$ represents the brain images, here $c = 1,2,\ldots,C$ and C indicates the image count.

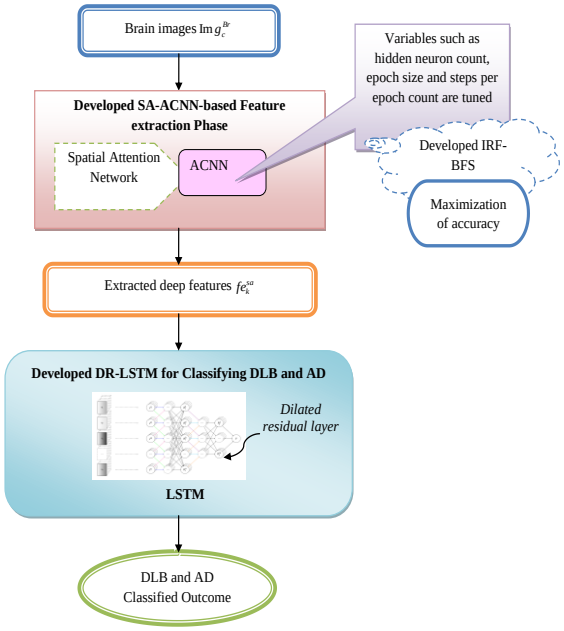

Fig. 1. Pictorial representation of the proposed DLB and AD imaging classification system.

TABLE II. DESCRIPTION OF THE INPUT IMAGE DATASET

Dataset name	Dataset link	Dataset description
Dataset1 (FDATA ADNI DATASET)	https://www.kaggle.com/datasets/ahmedashrafahmed/fdata-adni-dataset.	This dataset consists of 33,984 records, with 6,000 records selected for use. These 6,000 records are divided into training and testing sets, with 4,500 used for training and 1,500 for testing. The dataset is categorized into four classes, each with 1,500 records: CN (Cognitively Normal), LMCI (Late Mild Cognitive Impairment), AD, and EMCI (Early Mild Cognitive Impairment), where LMCI and EMCI comes under the category of DLB.

IV. SPATIAL ATTENTION BASED ADAPTIVE CONVOLUTION NEURAL NETWORK FOR CINGULATE ISLAND SIGN FEATURE EXTRACTION

A. Convolution Neural Network

The convolutional layer is a crucial part of feature extraction in a Convolutional Neural Network (CNN) [26], which employs certain hidden layers. CNN contains more than two hidden layers, and these layers interpret the image as a tensor, automatically extracting features and performing eventual categorization from input data. The usual CNN layers are as follows:

Input layer: The width, length, and number of channels, or their transformations, constitute the input tensor, which determines the size of the input layer, which contains the image information.

Convolutional layer: Transformation layers are those that imply the warping process from the preceding layer. This layer gathers the training outcome's weights or parameters. Usually smaller in width and length than the input layer, the output of this layer is a tensor known as a feature map, with a depth dimension. This layer aids in storing the training weight, which is represented by Eq. (1).

$$E_{wx} = \left(k1 * k2 * E_{PZ} * E_{QW} + E_{MF}\right) \quad (1)$$

Here, the kernel size is represented with the terms $k1$ and $k2$.

Pooling layer-This layer helps in reducing the size of the previous layer to identify the important features from the input tensor. The output dimension is determined by the kernel size; for instance, with a kernel size of two, the output dimension is divided. Fig. 2 illustrates the pictorial representation of a CNN for feature extraction process.

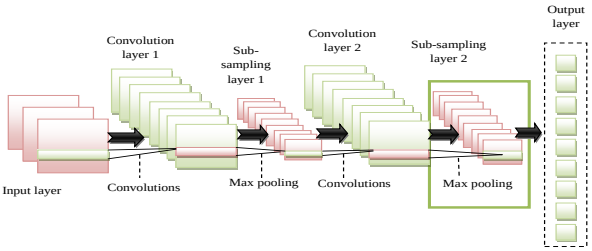

Fig. 2. Diagrammatic representation of CNN for feature extraction process.

B. Developed SA-ACNN-Based CIS Feature Extraction

Initially, the input brain images $Im\,g_c^{Br}$ are given for the feature extraction phase. The SA-ACNN utilizes spatial attention mechanisms to focus on the most relevant areas of medical images, such as lesions or other distinguishing patterns, enhancing the accuracy of feature extraction. This ability to prioritize important image regions allows the network to more effectively differentiate between DLB and AD. To further refine this process, IRF-BFS is applied to optimize the attributes of SA-ACNN. The parameters such as steps per epoch count, hidden neuron count, and epoch size in SA-ACNN are optimized to maximize the accuracy. Thus, it ensures that only the most relevant features are extracted for accurate diagnosis, with SA-ACNN focusing on key image areas. Finally, the CIS features are extracted which means neuro imaging features seen on DLB. The extracted features are represented with the term fe_k^{sa}.

CIS-based feature processing: In the process of differentiating DLB and AD, the model integrates Grad-CAM (Gradient-weighted Class Activation Mapping) to offer a deeper understanding of how the deep learning network reaches its diagnostic conclusions. Grad-CAM is a powerful visualization tool that helps to highlight which areas of the input image are most influential in the model's final predictions. Grad-CAM is specifically employed to locate and emphasize the CIS. This feature enables both clinicians and researchers to visually track the model's focus during the DLB–AD classification process. For images of DLB patients, Grad-CAM frequently highlights the CIS, demonstrating that the model places significant emphasis on this feature to differentiate DLB from AD. As the model continues to learn, its focus on the CIS becomes more pronounced and localized. When the CIS appears more prominently, the model assigns higher confidence to the DLB diagnosis, while images with

lower CIS ratios, suggesting the presence of AD pathology, lead to reduced confidence in DLB classification. The description of the spatial attention mechanism is provided below.

The spatial attention [27], [28] refers to a process that focuses on areas of input (usually images or sequences) that are most pertinent to the task at hand. When the model is creating predictions or extracting features, it uses this type of attention mechanism to help it prioritize geographic locations in the incoming images. Eq. (2) and Eq. (3) illustrate how the spatial attention mechanism is calculated.

$$F = N_f . \sigma \left(\left(v_i^{(y-1)} R_1 \right) R_2 (R_3 v_p^{(y-1)})^U + m_f \right) \quad (2)$$

$$F'_{p,l} = \frac{exp(F_{p,l})}{\sum_{l=1}^{Z} exp(F_{p,l})} \quad (3)$$

Here, the input of the y^{th} spatial block is signified with the term $v_i^{(y-1)}$ and the channels in the input images are specified with the term B_{y-1}. The learnable parameters are represented with the terms N_f and m_f and the term σ is utilized as the activation function. The element $F'_{p,l}$ in F signifies the semantic correlation strength between node p and node l. The diagrammatic representation of the developed SA-ACNN-based CIS Feature Extraction is presented in Fig. 3.

C. Parameter Optimization with IRF-BFS

The BFS algorithm is selected in this model as it offers several advantages, including efficient global search capabilities, simplicity, adaptability to various optimization problems, parallelism, and a good balance between exploration and exploitation. However, BFS also has some drawbacks, such as limited exploration of the search space, premature convergence and sensitivity to parameter tuning. These disadvantages can be addressed by using the IRF-BFS, which avoids randomness in the search space by updating the random variables to make accurate solution for the search process.

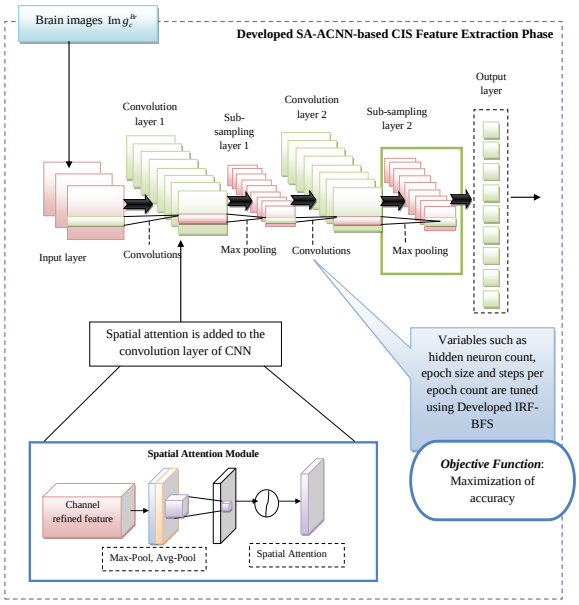

Fig. 3. Graphical representation of the implemented SA-ACNN-based CIS feature extraction.

IRF-BFS overcome premature convergence by adding diversity to the search, improving exploration, and minimizing the risk of getting stuck in local optima. Additionally, IRF-BFS reduces the dependency on manually tuning parameters by adapting them during the search. In this improved IRF-BFS approach, the random variable f is upgraded utilizing Eq. (4).

$$f = \frac{c_f}{\frac{a}{b}} \quad (4)$$

$$a = \frac{b_f}{c_f + w_f} \quad (5)$$

$$b = \frac{c_f + w_f}{b_f} \quad (6)$$

Here, the current fitness value is signified with the term c_f, the mean fitness value is signified with the term m_f, the worst fitness value is specified with the term w_f, and the best fitness value is represented with the term b_f. The pseudocode of the IRF-BFS is given in Algorithm 1.

Algorithm 1: Developed IRF-BFS

Set the values for the parameters: population Z and maximum iteration Max_{ite}

While $(ite \leq Max_{ite})$ do

- Update random variable $\boldsymbol{f}$ that is computed in Eq. (4)
- Perform flying search behavior
  - Estimate the new location of the bird in flying search region
- Perform Territorial behavior
  - Determine the new territory bird's position
  - Estimate the fitness function
  - Determine the new incursion birds' position
- If the position of the leading bird is superior to that of all other birds
  - Execute the role change mechanism
- End if
  - Examine the border
  - Estimate the fitness function
  - Upgrade M_p with M_p^{ite+1}

$$ite = ite + 1$$

End while

Output

Output

D. Objective Function of IRF-BFS-SA-ACNN Model

In the developed IRF-BFS-SA-ACNN-based feature extraction model, IRF-BFS is applied to optimize the attributes of SA-ACNN. The parameters such as steps per epoch count, hidden neuron count, and epoch size are optimized to maximize accuracy. The objective function of the developed IRF-BFS-SA-ACNN is expressed mathematically in Eq. (7).

$$Obj = \underset{\left\{Hdd_i^{cnn}, Eoo_j^{cnn}, Spe_k^{cnn}\right\}}{argmax} (acc) \quad (7)$$

Here, the term accindicates the accuracy, the term Spe_k^{cnn} denotes the steps per epoch count in the CNN with range of [500,1000], the term Eoo_j^{cnn} represents the epoch size with the range of [5,50] and the term Hdd_i^{cnn}signifies the hidden neuron count in the CNN with the range of [5,255].

The accuracy acc is a measure of how often a method accurately forecasts an outcome and it is derived in Eq. (8).

$$acc = \frac{(ka+en)}{(ka+en+s\square+ik)} \quad (8)$$

Here, the termkadenotes the true positive, en indicates the true negative, sh denotes the false positive, ik denotes the false negative values.

V. Dilated Residual-Long Short Term Memory for Differentiating Dementia with Lewy Bodies and Alzheimer's Disease

A. Long Short Term Memory

A memory element could replace each hidden element in the LSTM [29] . Each memory element is made up of different parts including input, output, forget, and internal states. The operation of the input and reset gate is achieved by Eq. (9) and Eq. (10).

$$m_d = \sigma\left(V_{bg} i_d + V_{lz} z_{d-1} + b_b\right) \quad (9)$$

$$j_d = \sigma\left(V_{ji} i_d + V_{zj} z_{d-1} + b_j\right) \quad (10)$$

The operation of the cell state and output gate is expressed by Eq. (11) and Eq. (12).

$$g_d = j_d \Theta g_{d-1} + l_d \Theta k\left(V_{gi} i_d + V_{gz} z_{d-1} + b_g\right) \quad (11)$$

$$t_d = \sigma\left(V_{wg} i_k + V_{wz} z_{k-1} + b_w\right) \quad (12)$$

The hidden state and memory state is attained in Eq. (13) and Eq. (14).

$$z_d = w_d \Theta p(g_d) \quad (13)$$

$$z_a = X_{zn} n_a + b_z \quad (14)$$

Here, the terms g_{d-1},$j_d$denotes the internal state, a forget gate, the terms m_d and t_d denotes an input gate, an output gate, the term V represents the weight matrix, the term σ represents the logistic sigmoid function, element-wise multiplication is denoted by the symbol Θ, z represents cell result activation point, the term $b$indicates bias, the term i and c indicates the input point and output point, and the terms $k$and $p$indicates the $tanh$activation operations, accordingly.

B. Dilated Residual-LSTM for Classifying DLB and AD

The extracted CIS features fe_k^{sa} are provided into the classification phase. The developed DR-LSTM helps to perform the differentiation process of DLB and AD by accurately identifying specific clinical features. It combines the strengths of dilated convolutions and residual layer networks. Dilated convolutions expand the receptive field, enabling the model to capture multi-scale contextual data, which is crucial for identifying subtle, long-range dependencies in disease progression. This combination of dilated convolution and residual layers improves the ability of the model to represent and track the evolving clinical features of DLB and AD, improving diagnostic accuracy. This integrated approach leads to a more robust and precise diagnostic process, ultimately aiding in the early and effective therapeutic intervention for these neurodegenerative diseases.

A residual block [30] is a fundamental component of residual network architecture. It is developed to mitigate the vanishing gradient issue and make training deep networks more feasible. The residual block can be mathematically indicated in Eq. (15).

$$i = H\left(v, \{R_p\}\right) + v \quad (15)$$

Here, the term $v$signifies the input of the residual block; the term $H\left(v, \{R_p\}\right)$indicates the residual mapping.

Dilated convolutions [32] are commonly used in models where capturing long-range dependencies is crucial and they allow the model to maintain high resolution while increasing the receptive field. This method is particularly advantageous in scenarios where traditional convolutions would result in excessive computation or loss of resolution due to down sampling. The function for a convolution can be computed using Eq. (16).

$$i(u) = \sum_{p=0}^{a} v(u + p.g).r(p) \quad (16)$$

Here, the term $r(p)$represents the weight at the index$p$, the term $g$represents the dilation factor, and $a$indicates the filter dimension. Finally, the classified outcome is obtained for identifying the DLB and AD classes. Fig. 4 represents the pictorial representation of developed DR-LSTM for Classifying DLB and AD.

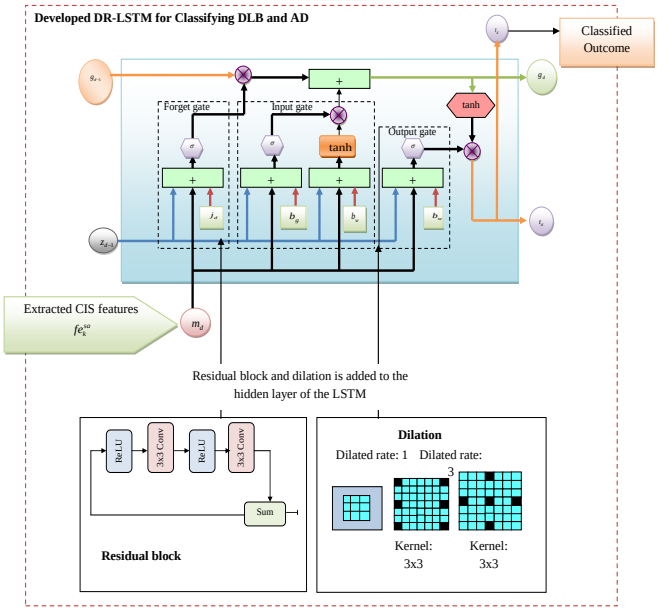

Fig. 4. Diagrammatic illustration of the developed DR-LSTM for classifying DLB and AD.

VI. Experimental Results

A. Resultant Feature Images by Varying Iteration

The developed DLB and AD Imaging Classification system was implemented utilizing Python. While developing the network, a maximum iteration of 50, a chromosome length of 3, and populations of 10, was considered. Fig. 5 provides the resultant feature images of the developed SA-ACNN by varying iteration.

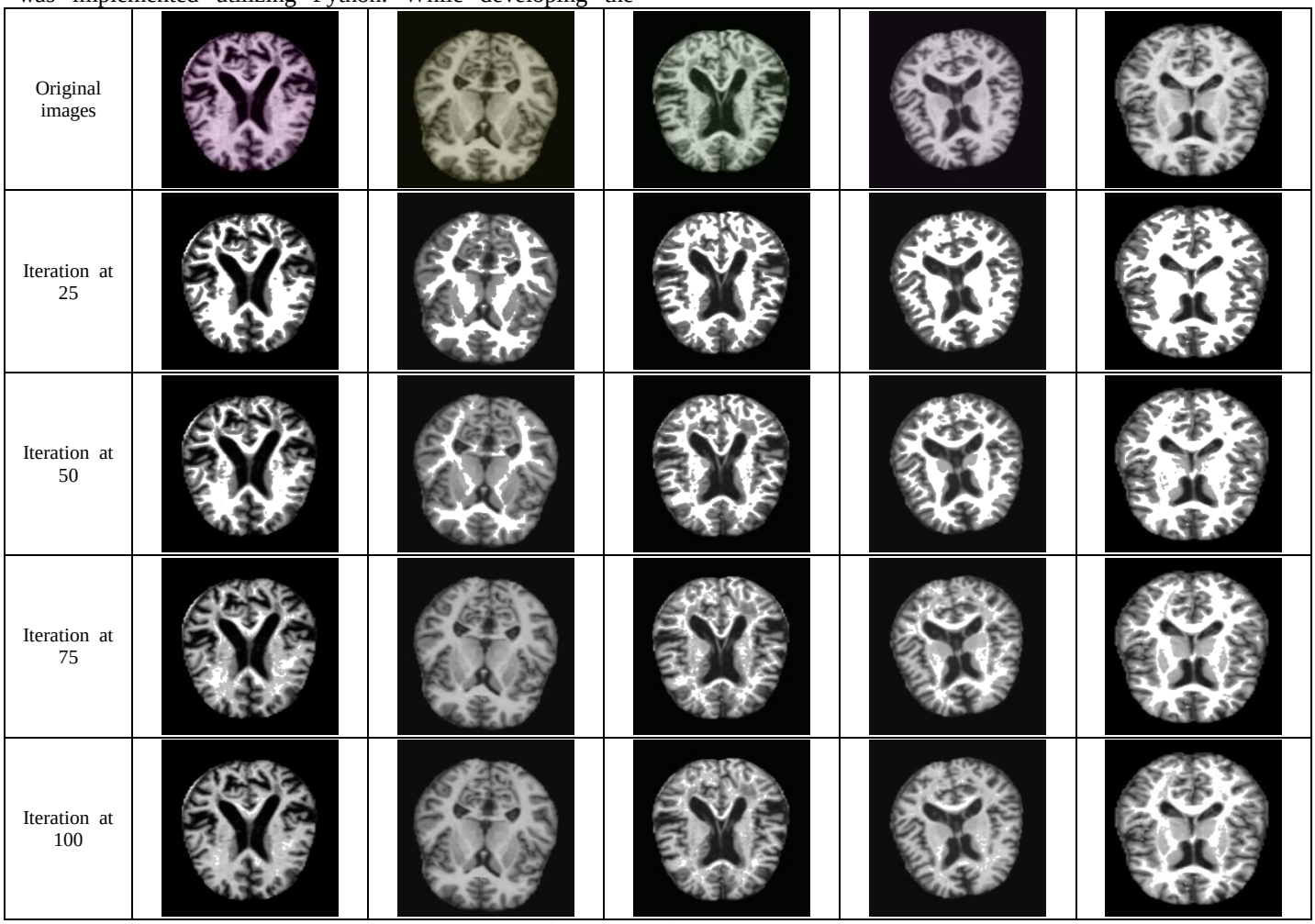

Fig. 5. Resultant feature images from the developed SA-ACNN.

B. Training and Testing Progress

The training progress graph is used to visualize the performance of a machine learning model during training and testing periods. This graph is a plot of the testing accuracy and testing loss over 1000 epochs. Fig. 6 and Fig. 7 provide the training progress graphs for the developed method. In Fig. 8 and Fig. 9, the testing accuracy increased rapidly, indicating that the model is learning and improving. However, after around 100 epochs, the accuracy fluctuates and stabilizes with some noise. The fluctuations suggest that the model's performance varies slightly with each epoch. In testing, the loss minimizes rapidly, showing that the model is learning to make better predictions. After around 100 epochs, the decrease in loss slows down and eventually stabilizes, showing minor reductions. The constant loss model suggests that a point has been reached where further training will not significantly improve performance.

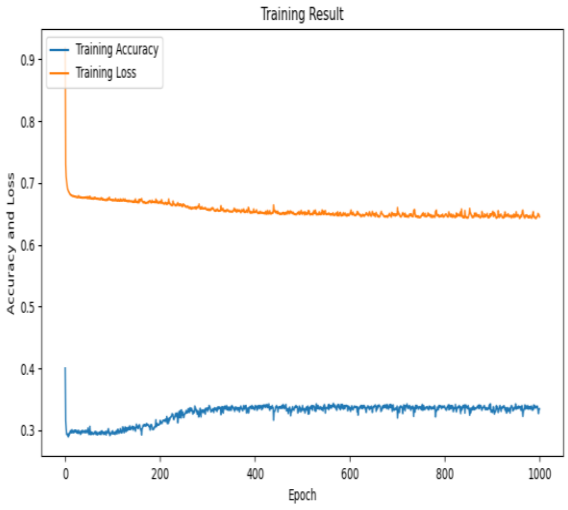

Fig. 6. Training accuracy of CNN model.

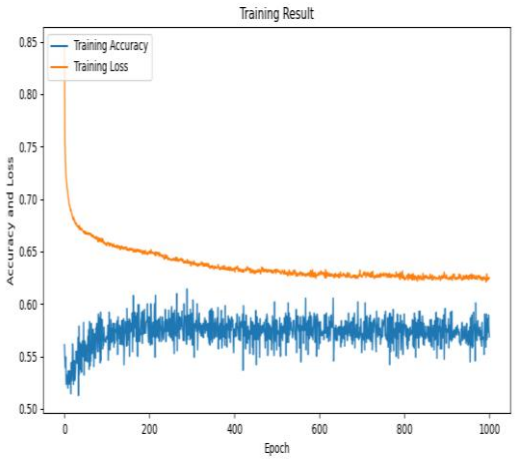

Fig. 7. Training accuracy of LSTM model.

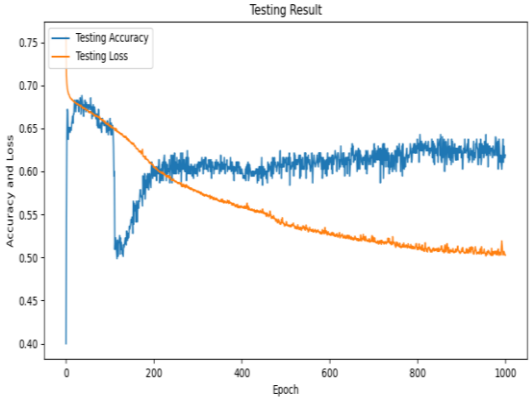

Fig. 8. Testing accuracy of CNN model.

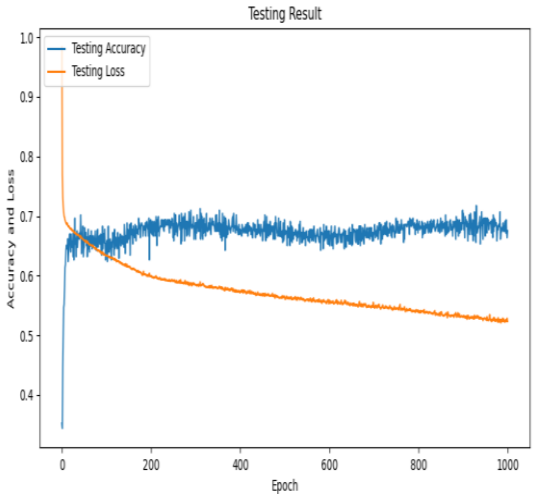

Fig. 9. Testing accuracy of CNN model.

C. Correlation Analysis

This statistical method assesses the strength and direction of the relationship between two continuous variables. Here, the black line represents a linear regression model, fitting the data points, which indicates a trend that supports this positive relationship. This type of analysis provides evidence that the features extracted by the SA-ACNN (i.e., the CIS ratio) are relevant for distinguishing between DLB and AD. It supports the effectiveness of the model in capturing clinically meaningful data that can be linked to the disease's severity or progression. Fig. 10 represents the correlation analysis of the developed SA-ACNN-based feature extraction model between AD and DLB classes.

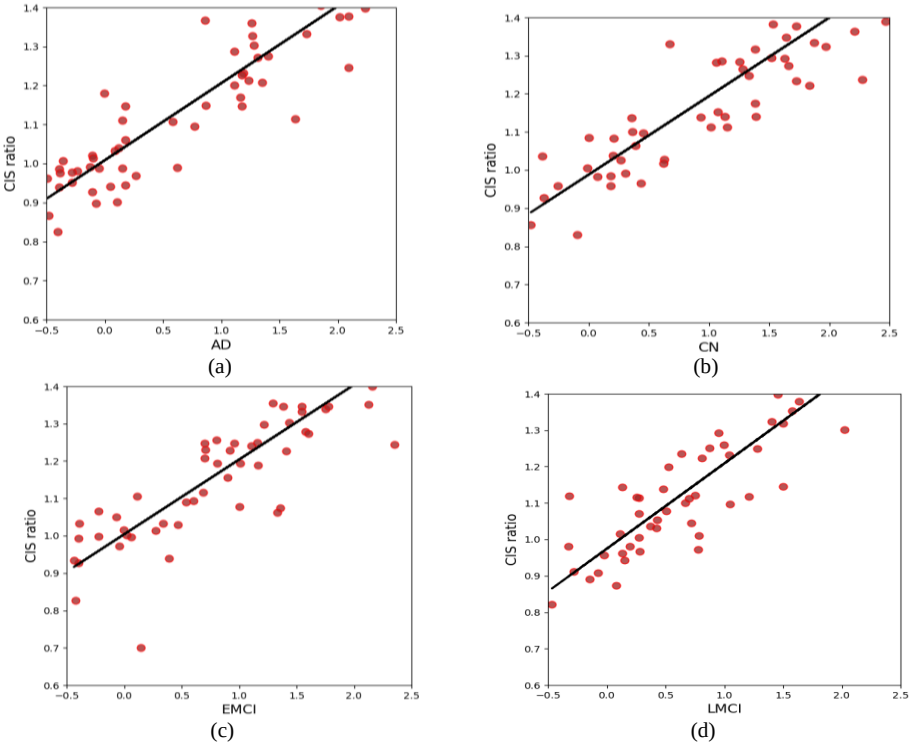

Fig. 10. Correlation analysis of the developed SA-ACNN-based Feature Extraction Model regarding different classes (a) AD, (b) CN, (c) EMCI, and (d) LMCI.

VII. Comparative Analysis and Discussion

A. Batch Size-Based Performance Analysis of Proposed Classification Model

The batch size-based performance analysis evaluates how different models perform on a given task by testing them on various batch sizes and evaluating metrics such as accuracy, MCC, CSI, FPR, FDR, precision. In Fig. 11(a), the accuracy of the developed AD-DLB-DNet framework outperforms RAN,

SVM, CNN-GCN, and CNN by 11.76%, 6.74%, 13.09%, and 3.26% in batch size-4, correspondingly. Thus, it is noted that the introduced DR-LSTM provides better performance than other classification techniques. Fig. 11 provides performance analysis by varying batch sizes.

B. ROC Analysis

Receiver Operating Characteristic (ROC), which is a metric, utilized to estimate the execution of a classification model, such as the DLB and AD differentiation model. The techniques compared, including RAN, SVM, CNN-GCN, CNN, and AD-DLB-DNet, all exhibit powerful performances. However, AD-DLB-DNet appears to have a slight edge over the others, making it a potentially more reliable choice for differentiating AD and DLB in clinical settings. Fig. 12 offers the ROC graph analysis of the proposed network.

C. Convergence Analysis

Convergence analysis refers to the study of how well the model's performance improves as the number of training iterations or epochs increases. The effectiveness of the implemented framework was estimated by comparing with several heuristic algorithms like Dwarf Mongoose Optimization (DMO) [31], Sparrow Search Algorithm (SSA) [32], Dingo Optimization Algorithm (DOA) [33], Birds Foraging Search (BFS) [34], and classifiers like RAN [35] , SVM, CNN-GCN, and CNN.

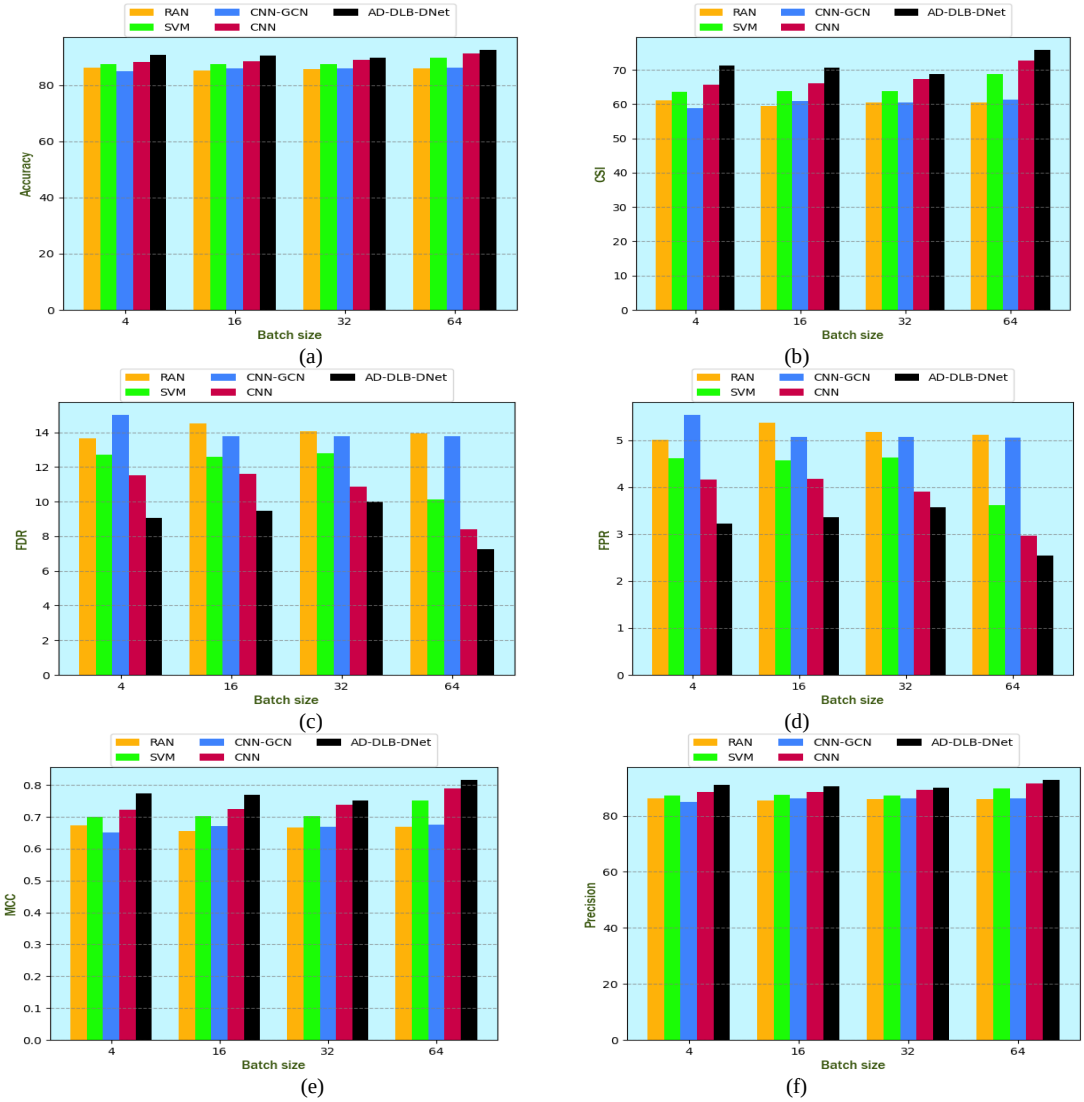

Fig. 11. Batchsize-based performance analysis of the developed method regarding (a) Accuracy, (b) CSI, (c) FDR, (d) FPR, (e) MCC, (f) Precision.

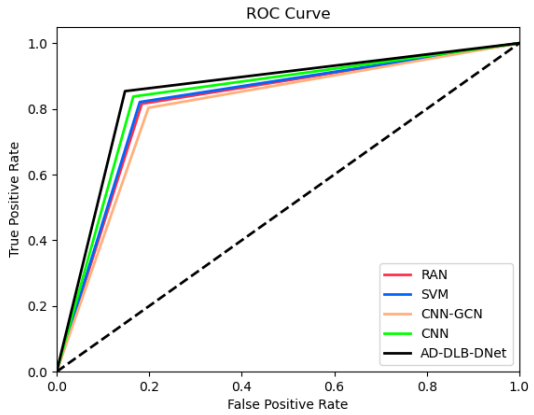

Fig. 12. ROC analysis of the developed technique.

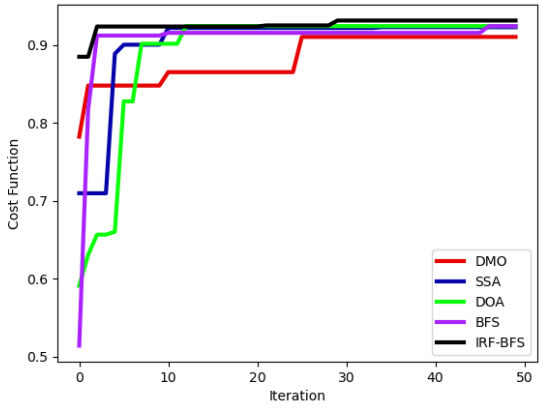

Fig. 13. Convergence analysis of the proposed technique.

At 10th iteration, the developed IRF-BFS approach performs better than the existing algorithms like DMO, SSA, DOA, and BFS by 13.63%, 11.11%, 12.35%, and 8.69%. By performing convergence analysis, researchers can develop a robust and accurate model for differentiating DLB and AD, ultimately improving diagnostic accuracy and patient outcomes. Fig. 13 provides the convergence analysis of the developed framework.

D. Confusion Matrix of the Classification Model

The confusion matrix is a commonly used performance measurement tool in classification issues. It compares a model's classified classes with the actual ground truth labels, to assess how well the system performs. Moreover, it helps to identify areas where the model performs well and where improvements are needed. Consequently, it shows how well the model can differentiate between AD and DLB, particularly by analyzing how often the model misclassifies one disease as another. Fig. 14 provides the confusion matrix of the developed model.

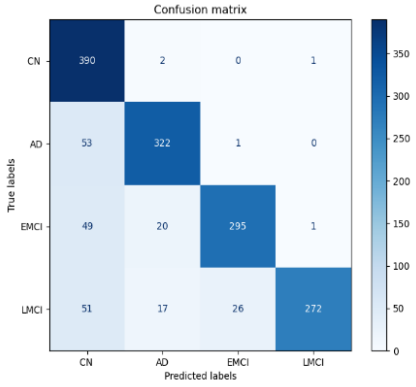

Fig. 14. Confusion matrix of the proposed classification model.

E. Comparative Analysis with K-Fold Cross Vadildation

Comparative Analysis of the Proposed Classification model is always needed to analyze the effectiveness of the developed model. K-fold cross-validation analysis refers to a method that is utilized to assess the effectiveness of a model, especially in cases where you want to ensure your method generalizes well with new information. K-fold analysis is used to evaluate effectively how the model distinguishes between the two diseases. In the below Table III, it is clearly shown that the developed AD-DLB-DNet system, in terms of accuracy, is better in performance than the existing methods such as RAN, SVM, CNN-GCN, and CNN by 4.27%, 2.85%, 3.26%, and 1.988%, respectively. AD-DLB-DNet consistently outperforms the other models with the highest accuracy of 92.104%, specificity of 97.215, F1 Score of 85.361, MCC value 0.804, and CSI value 74.461, while also maintaining the lowest FPR of 2.785 and FDR of 7.917 at K-Fold-5. This suggests that AD-DLB-DNet is the most robust model for differentiating between DLB and AD. Table III shows the Comparative K-fold analysis of the developed framework.

TABLE III. COMPARATIVE K-FOLD ANALYSIS OF THE PROPOSED METHOD WITH EXISTING METHODS

TERMS	RAN [30]	SVM [2]	CNN-GCN [3]	CNN [7]	AD-DLB-DNet
K-Fold-1					
Accuracy	87.750	88.958	88.604	90.604	91.500
Specificity	95.664	96.013	95.910	96.680	96.969
FPR	4.336	3.987	4.090	3.320	3.031
FDR	11.917	11.083	11.333	9.333	8.583
F1	78.238	80.105	79.551	82.832	84.320
MCC	0.707	0.733	0.725	0.770	0.790
CSI	64.255	66.813	66.046	70.695	72.890
K-Fold-2					

Accuracy	84.708	87.688	85.750	89.146	91.833
Specificity	94.338	95.494	94.724	96.134	97.121
FPR	5.662	4.506	5.276	3.866	2.879
FDR	15.250	12.417	14.333	10.750	8.167
F1	73.483	78.054	75.036	80.436	84.900
MCC	0.641	0.704	0.663	0.737	0.798
CSI	58.081	64.007	60.047	67.274	73.762
K-Fold-3					
Accuracy	85.896	87.021	86.563	88.583	90.708
Specificity	94.790	95.450	95.087	95.826	96.740
FPR	5.210	4.550	4.913	4.174	3.260
FDR	14.167	12.417	13.417	11.583	9.167
F1	75.265	77.138	76.313	79.476	83.016
MCC	0.666	0.692	0.680	0.724	0.772
CSI	60.340	62.784	61.698	65.942	70.964
K-Fold-4					
Accuracy	85.500	85.813	83.771	89.229	89.229
Specificity	94.732	94.701	94.009	96.139	96.167
FPR	5.268	5.299	5.991	3.861	3.833
FDR	14.250	14.417	16.000	10.750	10.667
F1	74.728	75.101	72.129	80.557	80.571
MCC	0.659	0.664	0.622	0.739	0.739
CSI	59.652	60.129	56.407	67.443	67.464
K-Fold-5					
Accuracy	86.500	88.667	87.854	90.500	92.104
Specificity	95.082	95.969	95.643	96.647	97.215
FPR	4.918	4.031	4.357	3.353	2.785
FDR	13.417	11.167	12.000	9.417	7.917
F1	76.229	79.671	78.367	82.662	85.361
MCC	0.679	0.727	0.709	0.767	0.804
CSI	61.589	66.211	64.430	70.447	74.461

VIII. CONCLUSION

This study aimed to differentiate DLB from AD using a deep learning model. The process began with collecting the necessary images from a benchmark dataset. The images were fed into the SA-ACNN for CIS feature extraction. Using Grad-CAM, the deep learning model not only provides accurate predictions for distinguishing DLB from AD but also offers a clear visual representation of the CIS as an essential feature for DLB diagnosis. This visualization technique enhances the model's interpretability, fostering greater trust in its decision-making process. To perform differentiation, a DR-LSTM was proposed, which effectively identified clinical features. This comprehensive model aimed to enhance the differential diagnosis of DLB as well as AD, facilitating more effective therapeutic measures. Finally, validation steps were performed to confirm the efficacy of the method that ensures its reliability in clinical settings. The accuracy of the developed AD-DLB-DNet framework is more effective than RAN, SVM, CNN-GCN, and CNN by 8.41%, 4.72%, 7.09%, and 3.01%, respectively at the k-fold value to be 2. The suggested model is used for the differentiation of DLB and AD for taking effective therapeutic measures. The present study faces limitations such as data constraints, generalization challenges, and the need for extensive clinical validation to ensure reliability and ethical compliance. In future work, several avenues can be explored to improve the differentiation of DLB and AD utilizing deep learning models. Expanding the dataset to include more diverse images from various demographics and medical conditions can improve model robustness.

REFERENCES

[1] V. Vimbi, N. Shaffi, and M. Mahmud, "Interpreting artificial intelligence models: a systematic review on the application of LIME and SHAP in Alzheimer's disease detection," Brain Inform, vol. 11, no. 1, p. 10, Dec. 2024, doi: 10.1186/s40708-024-00222-1.

[2] B. Lei et al., "Hybrid federated learning with brain-region attention network for multi-center Alzheimer's disease detection," Pattern

Recognit, vol. 153, p. 110423, Sep. 2024, doi: 10.1016/j.patcog.2024.110423.

[3] N. Pradhan, S. Sagar, and A. S. Singh, "Analysis of MRI image data for Alzheimer disease detection using deep learning techniques," Multimed Tools Appl, vol. 83, no. 6, pp. 17729–17752, Jul. 2023, doi: 10.1007/s11042-023-16256-2.

[4] S. M. Mahim et al., "Unlocking the Potential of XAI for Improved Alzheimer's Disease Detection and Classification Using a ViT-GRU Model," IEEE Access, vol. 12, pp. 8390–8412, 2024, doi: 10.1109/ACCESS.2024.3351809.

[5] M. Trinh, R. Shahbaba, C. Stark, and Y. Ren, "Alzheimer's disease detection using data fusion with a deep supervised encoder," Frontiers in Dementia, vol. 3, Feb. 2024, doi: 10.3389/frdem.2024.1332928.

[6] D. M. O'Shea et al., "Practical use of DAT SPECT imaging in diagnosing dementia with Lewy bodies: a US perspective of current guidelines and future directions," Front Neurol, vol. 15, Apr. 2024, doi: 10.3389/fneur.2024.1395413.

[7] M. J. Plastini et al., "Multiple biomarkers improve diagnostic accuracy across Lewy body and Alzheimer's disease spectra," Ann Clin Transl Neurol, vol. 11, no. 5, pp. 1197–1210, May 2024, doi: 10.1002/acn3.52034.

[8] N. S. Sjaelland, M. H. Gramkow, S. G. Hasselbalch, and K. S. Frederiksen, "Digital Biomarkers for the Assessment of Non-Cognitive Symptoms in Patients with Dementia with Lewy Bodies: A Systematic Review," Journal of Alzheimer's Disease, vol. 100, no. 2, pp. 431–451, Jul. 2024, doi: 10.3233/JAD-240327.

[9] J. Levin et al., "α - Synuclein seed amplification assay detects Lewy body co - pathology in autosomal dominant Alzheimer's disease late in the disease course and dependent on Lewy pathology burden," Alzheimer's & Dementia, vol. 20, no. 6, pp. 4351‐4365, Jun. 2024, doi: 10.1002/alz.13818.

[10] K. Sravani and V. RaviSankar, "Intelligent Differentiation Framework for Lewy Body Dementia and Alzheimer's disease using Adaptive Multi-Cascaded ResNet–Autoencoder–LSTM Network," Int J Image Graph, Apr. 2024, doi: 10.1142/S0219467825500664.

[11] H. Sohrabnavi, M. Mohammadimasoudi, and H. Hajghassem, "Early detection of Alzheimer's disease by measuring amyloid beta-42 concentration in human serum based on liquid crystals," Sens Actuators B Chem, vol. 401, p. 134966, Feb. 2024, doi: 10.1016/j.snb.2023.134966.

[12] Y. Zeng, Z. Huang, Y. Liu, and T. Xu, "Printed Biosensors for the Detection of Alzheimer's Disease Based on Blood Biomarkers," J Anal Test, vol. 8, no. 2, pp. 133–142, Jun. 2024, doi: 10.1007/s41664-023-00277-9.

[13] M. J. Armstrong, D. J. Irwin, J. B. Leverenz, N. Gamez, A. Taylor, and J. E. Galvin, "Biomarker Use for Dementia With Lewy Body Diagnosis," Alzheimer Dis Assoc Disord, vol. 35, no. 1, pp. 55–61, Jan. 2021, doi: 10.1097/WAD.0000000000000414.

[14] S. Siuly, Ö. F. Alçin, H. Wang, Y. Li et al., "Exploring Rhythms and Channels-Based EEG Biomarkers for Early Detection of Alzheimer's Disease," IEEE Trans Emerg Top Comput Intell, vol. 8, no. 2, pp. 1609–1623, Apr. 2024, doi: 10.1109/TETCI.2024.3353610.

[15] B. TaghiBeyglou and F. Rudzicz, "Context is not key: Detecting Alzheimer's disease with both classical and transformer-based neural language models," Natural Language Processing Journal, vol. 6, p. 100046, Mar. 2024, doi: 10.1016/j.nlp.2023.100046.

[16] I. Bazarbekov, A. Razaque, M. Ipalakova et al., "A review of artificial intelligence methods for Alzheimer's disease diagnosis: Insights from neuroimaging to sensor data analysis," Biomed Signal Process Control, vol. 92, p. 106023, Jun. 2024, doi: 10.1016/j.bspc.2024.106023.

[17] J. Therriault et al., "Comparison of immunoassay- with mass spectrometry-derived p-tau quantification for the detection of Alzheimer's disease pathology," Mol Neurodegener, vol. 19, no. 1, p. 2, Jan. 2024, doi: 10.1186/s13024-023-00689-2.

[18] T. Nakata et al., "Differential diagnosis of MCI with Lewy bodies and MCI due to Alzheimer's disease by visual assessment of occipital hypoperfusion on SPECT images," Jpn J Radiol, vol. 42, no. 3, pp. 308–318, Mar. 2024, doi: 10.1007/s11604-023-01501-3.

[19] S. M. S. Karim, M. S. Fahad, and R. S. Rathore, "Identifying discriminative features of brain network for prediction of Alzheimer's disease using graph theory and machine learning," Front Neuroinform, vol. 18, Jun. 2024, doi: 10.3389/fninf.2024.1384720.

[20] M. E. Hasan and A. Wagler, "New Convolutional Neural Network and Graph Convolutional Network-Based Architecture for AI Applications in Alzheimer's Disease and Dementia-Stage Classification," AI, vol. 5, no. 1, pp. 342–363, Feb. 2024, doi: 10.3390/ai5010017.

[21] K. Etminani et al., "A 3D deep learning model to predict the diagnosis of dementia with Lewy bodies, Alzheimer's disease, and mild cognitive impairment using brain 18F-FDG PET," Eur J Nucl Med Mol Imaging, vol. 49, no. 2, pp. 563–584, Jan. 2022, doi: 10.1007/s00259-021-05483-0.

[22] L. Gjerum et al., "A visual rating scale for cingulate island sign on 18F-FDG-PET to differentiate dementia with Lewy bodies and Alzheimer's disease," J Neurol Sci, vol. 410, p. 116645, Mar. 2020, doi: 10.1016/j.jns.2019.116645.

[23] H. Kanetaka et al., "Differentiating Mild Cognitive Impairment, Alzheimer's Disease, and Dementia With Lewy Bodies Using Cingulate Island Sign on Perfusion IMP-SPECT," Front Neurol, vol. 11, Nov. 2020, doi: 10.3389/fneur.2020.568438.

[24] B. Y. Lim et al., "Deep Learning Model for Prediction of Progressive Mild Cognitive Impairment to Alzheimer's Disease Using Structural MRI," Front Aging Neurosci, vol. 14, Jun. 2022, doi: 10.3389/fnagi.2022.876202.

[25] I. G. McKeith et al., "Diagnosis and management of dementia with Lewy bodies," Neurology, vol. 89, no. 1, pp. 88–100, Jul. 2017, doi: 10.1212/WNL.0000000000004058.

[26] S. Basheera and M. Satya Sai Ram, "A novel CNN based Alzheimer's disease classification using hybrid enhanced ICA segmented gray matter of MRI," Computerized Medical Imaging and Graphics, vol. 81, p. 101713, Apr. 2020, doi: 10.1016/j.compmedimag.2020.101713.

[27] C. Li, H. Zhang, Z. Wang, Y. Wu, and F. Yang, "Spatial-Temporal Attention Mechanism and Graph Convolutional Networks for Destination Prediction," Front Neurorobot, vol. 16, Jul. 2022, doi: 10.3389/fnbot.2022.925210.

[28] H. Wang et al., "A Residual LSTM and Seq2Seq Neural Network Based on GPT for Chinese Rice-Related Question and Answer System," Agriculture, vol. 12, no. 6, p. 813, Jun. 2022, doi: 10.3390/agriculture12060813.

[29] C. Chen, X. Lin, and G. Terejanu, "An Approximate Bayesian Long Short- Term Memory Algorithm for Outlier Detection," in 2018 24th International Conference on Pattern Recognition (ICPR), IEEE, Aug. 2018, pp. 201–206. doi: 10.1109/ICPR.2018.8545695.

[30] C. Tian, X. Zhu, Z. Hu, and J. Ma, "Deep spatial-temporal networks for crowd flows prediction by dilated convolutions and region-shifting attention mechanism," Applied Intelligence, vol. 50, no. 10, pp. 3057–3070, Oct. 2020, doi: 10.1007/s10489-020-01698-0.

[31] J. O. Agushaka, A. E. Ezugwu, and L. Abualigah, "Dwarf Mongoose Optimization Algorithm," Comput Methods Appl Mech Eng, vol. 391, p. 114570, Mar. 2022, doi: 10.1016/j.cma.2022.114570.

[32] J. Xue and B. Shen, "A novel swarm intelligence optimization approach: sparrow search algorithm," Systems Science & Control Engineering, vol. 8, no. 1, pp. 22–34, Jan. 2020, doi: 10.1080/21642583.2019.1708830.

[33] J. H. Almazán-Covarrubias, H. Peraza-Vázquez, A. F. Peña-Delgado, and P. M. García-Vite, "An Improved Dingo Optimization Algorithm Applied to SHE-PWM Modulation Strategy," Applied Sciences, vol. 12, no. 3, p. 992, Jan. 2022, doi: 10.3390/app12030992.

[34] Z. Zhang, C. Huang, K. Dong, and H. Huang, "Birds foraging search: a novel population-based algorithm for global optimization," Memet Comput, vol. 11, no. 3, pp. 221–250, Sep. 2019, doi: 10.1007/s12293-019-00286-1.

[35] A. Behera, Z. Wharton, Y. Liu, M. Ghahremani et al., "Regional Attention Network (RAN) for Head Pose and Fine-Grained Gesture Recognition," IEEE Trans Affect Comput, vol. 14, no. 1, pp. 549–562, Jan. 2023, doi: 10.1109/TAFFC.2020.3031841.